



Circular dichroism: electronic

Ingolf Warnke and Filipp Furche*

First-principles calculations of electronic circular dichroism (ECD) are widely used to determine absolute configurations of chiral molecules. In addition, ECD is a sensitive probe for the three-dimensional molecular structure, making ECD calculations a useful tool to study conformational changes. In this review, we explain the origin of ECD and optical activity using response theory. While the quantum-mechanical underpinnings of ECD have been known for a long time, efficient electronic structure methods for ECD calculations on molecules with more than 10–20 atoms have become widely available only in the past decade. We review the most popular methods for ECD calculation, focusing on time-dependent density functional theory. Although single-point vertical ECD calculations yield useful accuracy for conformationally rigid systems, inclusion of finite-temperature effects is necessary for flexible molecules. The scope and limitations of modern ECD calculations are illustrated by applications to helicenes, fullerenes, iso-schizozygane alkaloids, paracyclophanes, β -lactams, and transition metal complexes. © 2011 John Wiley & Sons Ltd.

How to cite this article:

WIREs Comput Mol Sci 2012, 2: 150–166 doi: 10.1002/wcms.55

INTRODUCTION

Circular dichroism (CD) is the difference between the absorption coefficients for left and right circularly polarized light,¹ ε_L and ε_R (see Figure 1),

$$\Delta\varepsilon = \varepsilon_L - \varepsilon_R. \quad (1)$$

$\Delta\varepsilon$ as a function of the incident light frequency ω is called CD spectrum. In this review, we focus on frequencies in the visible and ultraviolet (UV), where electronic excitations dominate.

Chirality is a necessary requirement for molecules and crystals to exhibit CD. The CD of pure enantiomers differs in sign, but not in magnitude. For example, Figure 2 shows the electronic circular dichroism (ECD) spectra of *trans*-(2S,3S)-dimethyloxirane and its enantiomer.^{2,3} There is no simple relation between the absolute configuration (AC) of an enantiomer and the sign of its ECD spectrum: CD depends on details of the electronic and geometric molecular structure. However, *ab initio* electronic structure calculations are nowadays able to predict ECD accurately and thus allow an assignment of the AC by comparison of experimental and

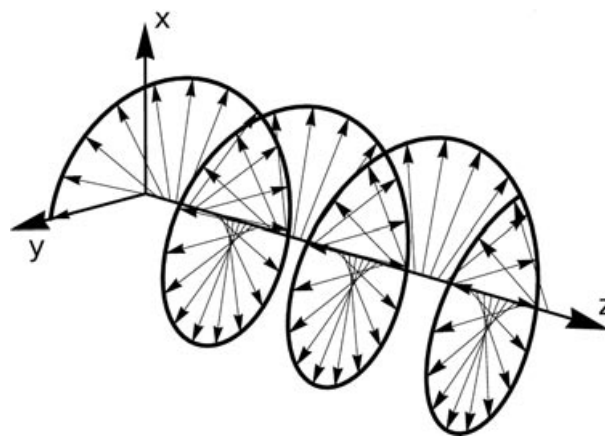


FIGURE 1 | Left-circularly polarized light propagating in z-direction. The plotted electric field vectors rotate in the x–y plane, describing a left-handed helix. The magnetic field vector (not shown) is perpendicular to the electric field vector.

computed ECD spectra. In the example of Figure 2, the AC of the experimental spectrum is assigned (2S,3S) by comparison to the computed ECD spectra. The assignment of ACs by computed ECD spectra is becoming increasingly popular because it is less expensive and faster than anomalous-dispersion X-ray diffraction^{4,5} and it does not require crystals. ECD-based determination of the AC can be complemented by calculations of the optical rotation (OR). As ECD

*Correspondence to: filipp.furche@uci.edu

Department of Chemistry, University of California, Irvine, CA, USA

DOI: 10.1002/wcms.55

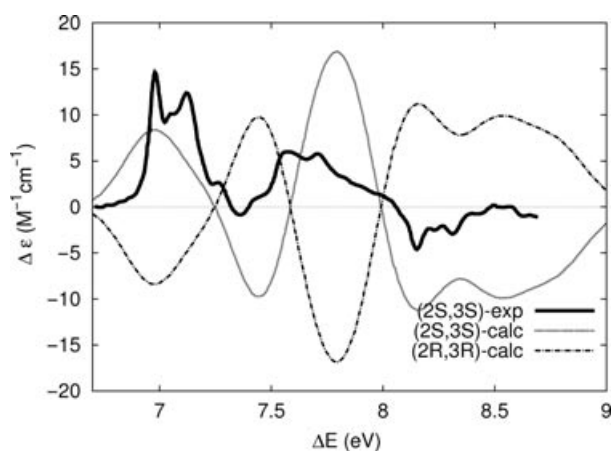


FIGURE 2 | Experimental ECD spectrum of *trans*-(2S,3S)-dimethyloxirane (solid) together with calculated ECD spectra³ of the (2S,3S) and the (2R,3R) enantiomers. (Theoretical data reprinted with permission from Ref 3. Copyright 2002 American Institute of Physics. Experimental data reprinted with permission from Ref 2. Copyright 1994 Elsevier.)

and OR are closely related, we will briefly comment on OR, but refer the reader to specialized reviews^{6–10} for details.

ECD spectra are much more sensitive to the three-dimensional molecular structure than ordinary absorption spectra because ECD intensities capture angular correlations between electric and magnetic transition moments. In biology, ECD spectra are frequently used to characterize the secondary structure of proteins.^{1,11–13} With accurate electronic structure ECD calculations becoming available for larger systems, it is possible to quantify the ECD-structure relation and infer details of the three-dimensional molecular structure such as conformation from ECD spectra. Many excellent books^{1,14–17} and reviews^{9,10,18,19} on ECD exist. The present paper focuses on recent developments in electronic structure methods for ECD. In the section *Basic Definitions*, we set the stage by reviewing basic quantities and relations underlying ECD. Section *Electronic Structure Methods for ECD* summarizes some of the most important methods presently available for ECD calculations. In the section *Applications*, we review instructive examples of ECD calculations.

BASIC DEFINITIONS

Electric Dipole–Magnetic Dipole Polarizability

Consider a molecule interacting with a monochromatic electromagnetic field oscillating at frequency ω . In the frequency domain, the first-order change in the

molecular electric dipole moment μ is

$$\mu_j^{(1)}(\omega) = \sum_k \alpha_{jk}(\omega) E_k(\omega) + \frac{i\omega}{c} \sum_k G_{jk}(\omega) B_k(\omega) + \sum_{kl} P_{jkl}(\omega) \frac{\partial E_k(\omega)}{\partial l} + \mathcal{O}\left(\frac{1}{\lambda^2}\right), \quad (2)$$

where $j, k, l \in (x, y, z)$. \mathbf{E} and \mathbf{B} denote the electric and magnetic field vectors at the position of the molecule. Atomic units (a.u.) are used throughout, unless otherwise stated. $\alpha_{jk}(\omega)$ is the well-known linear electric dipole–electric dipole polarizability. The linear electric dipole–magnetic dipole polarizability $G_{jk}(\omega)$ describes the linear response of the electric dipole moment induced by an oscillating magnetic field and is the central quantity in ECD spectroscopy. $P_{jkl}(\omega)$ is the electric dipole–quadrupole polarizability tensor. The magnetic dipole and electric quadrupole terms in Eq. (2) are of the same order in $\omega/c = 2\pi/\lambda$, where c is the velocity of light and λ is the wavelength of the incident radiation, but only the magnetic dipole term gives rise to ECD. In typical ECD measurements, the wavelength λ is large compared to the molecular dimensions, which justifies the neglect of higher-order multipoles in Eq. (2). Gas-phase and solution experiments capture only the isotropic average

$$G(\omega) = \frac{1}{3} \sum_j G_{jj}(\omega). \quad (3)$$

(See Ref 20 for recent work on the full electric dipole–magnetic dipole tensor.) First-order response theory yields the sum-over-state (SOS) expression for G at complex frequency z ,

$$G(z) = -\frac{c}{3} \sum_n \frac{1}{\Omega_{0n}} \times \left(\frac{R_{0n}}{z - \Omega_{0n} + i\eta} - \frac{R_{0n}}{z + \Omega_{0n} + i\eta} \right). \quad (4)$$

Here, $\Omega_{0n} = E_n - E_0$ denotes the excitation energy from the ground state Ψ_0 to the n th excited state Ψ_n , and R_{0n} is the rotatory strength of the corresponding transition.²¹ η is a small contour distortion making $G(z)$ analytical in the upper complex plane. This ensures causal behavior of the polarizability in the time domain.²² R_{0n} may be expressed in terms of the vectors of the electric transition dipole moment

$$\mu_{0n} = -\langle \Psi_n | \hat{\mathbf{r}} | \Psi_0 \rangle \quad (5)$$

and the magnetic transition dipole moment

$$\mathbf{m}_{0n} = -\frac{1}{2c} \langle \Psi_n | \hat{\mathbf{L}} | \Psi_0 \rangle, \quad (6)$$

where \hat{r} and \hat{L} are the position and the angular momentum operator, respectively. For real wavefunctions Ψ_0 and Ψ_n , the electric transition dipole moment $\boldsymbol{\mu}_{0n} = \boldsymbol{\mu}_{n0} = \boldsymbol{\mu}_{0n}^*$ is purely real, whereas the magnetic transition dipole moment $\mathbf{m}_{0n} = -\mathbf{m}_{n0} = -\mathbf{m}_{0n}^*$ is purely imaginary. The rotatory strength is the imaginary part of the scalar of the scalar product of $\boldsymbol{\mu}_{0n}$ and \mathbf{m}_{0n} ,

$$R_{0n} = \text{Im}[\boldsymbol{\mu}_{0n} \cdot \mathbf{m}_{0n}]. \quad (7)$$

Within the Born–Oppenheimer approximation, the molecular eigenstates Ψ_0 , Ψ_n are approximated by products of electronic and nuclear wavefunctions. To leading order in the Herzberg–Teller expansion, the electric and magnetic transition moments of an allowed transition separate into a purely electronic part and a Franck–Condon factor. Although the electronic part governs integrated intensities,¹⁸ the Franck–Condon factors determine the vibronic fine structure of ECD spectra and can affect band shapes significantly, as discussed in the section *Temperature Effects*. We will focus on the electronic part here and assume in the following that the states Ψ_0 , Ψ_n are solutions of the electronic Schrödinger equation.

Circular Dichroism

$G(z)$ may be decomposed into a real and an imaginary part. The imaginary part of G (at real frequency ω),

$$\text{Im}[G(\omega)] = \frac{c\pi}{3} \sum_n \frac{1}{\Omega_{0n}} (R_{0n}\delta(\omega - \Omega_{0n}) - R_{0n}\delta(\omega + \Omega_{0n})), \quad (8)$$

determines the shape of the linear ECD spectrum,¹⁸

$$\Delta\varepsilon(\omega) = \frac{N_A}{\ln 10} 16\pi\omega^2 \text{Im}[G(\omega)], \quad (9)$$

where N_A is Avogadro's constant and $\ln 10 = 2.302585\dots$ Equations (8) and (9) imply that the rotatory strength determines the integrated intensity of a single ECD band of width 2ε ,

$$R_{0n} = \frac{3\ln 10}{16\pi^2 c N_A} \int_{\Omega_{0n}-\varepsilon}^{\Omega_{0n}+\varepsilon} d\omega \frac{\Delta\varepsilon(\omega)}{\omega}. \quad (10)$$

The rotatory strength is usually expressed in 10^{-40} cgs units, where 1 a.u. corresponds to 64604.8×10^{-40} erg cm³. Rotatory strengths satisfy various sum rules.¹⁸ Most importantly, their sum is zero,²³

$$\sum_n R_{0n} = 0. \quad (11)$$

Optical Rotation

The real (dispersive) part of $G(z)$,

$$\beta(\omega) = \text{Re}[G(\omega)] = \frac{-2c}{3} \sum_n \frac{R_{0n}}{\omega^2 - \Omega_{0n}^2}, \quad (12)$$

is the optical rotatory dispersion (ORD). As first pointed out by Rosenfeld²¹ in 1929, the chiral response parameter $\beta(\omega)$ determines the specific rotation,

$$[\alpha]_\omega = C \frac{\omega^2}{M} \beta(\omega), \quad (13)$$

with M being the molar mass. If $[\alpha]_\omega$ is in $^\circ/(\text{dm}(\text{g}/\text{cm}^3))$, M in g/mol, and ω and β are in a.u., the value of the constant C is 6.469×10^3 (cf. Ref 24).

Because the real-time response of $\boldsymbol{\mu}$ is causal, $G(z)$ is analytic in the upper complex plane.²² Thus, Cauchy's theorem gives rise to Kramers–Kronig relations^{18,25–27} between $\text{Re}[G(\omega)]$ and $\text{Im}[G(\omega)]$:

$$\text{Re}[G(\omega)] = \frac{2}{\pi} P \int_0^\infty d\omega' \frac{\omega' \text{Im}[G(\omega')]}{\omega'^2 - \omega^2}, \quad (14)$$

$$\text{Im}[G(\omega)] = -\frac{2}{\pi} P \int_0^\infty d\omega' \frac{\omega' \text{Re}[G(\omega')]}{\omega'^2 - \omega^2}, \quad (15)$$

where P denotes the Cauchy principal value. Equations (13) and (14) show that knowledge of the entire ECD spectrum is equivalent to knowledge of the entire ORD curve. Figure 3 illustrates the qualitative behavior of $\text{Re}[G(\omega)]$ and $\text{Im}[G(\omega)]$ as a function of ω .

Selection Rules

A given electric transition has finite intensity in the ECD spectrum if the rotatory strength R_{0n} [Eq. (7)] is nonvanishing. This is possible only if the transition is spin-allowed and both the electric and magnetic transition dipole moments $\boldsymbol{\mu}_{0n}$ and \mathbf{m}_{0n} are nonzero. In addition, a necessary condition for a nonzero rotatory strength is that the scalar product $\boldsymbol{\mu}_{0n} \cdot \mathbf{m}_{0n}$ does not vanish on symmetry grounds.

The electric dipole moment operator transforms as a polar vector and the magnetic dipole moment operator transforms as an axial vector. Thus, for $\boldsymbol{\mu}_{0n}$ and \mathbf{m}_{0n} to be nonzero, polar and axial vectors must transform according to the same irreducible representations of the molecular point group. This is possible if the molecular point group does not contain improper rotations, i.e., mirror reflections, inversions, and higher S_n axes, because polar and axial vectors differ by a sign in their transformation properties under improper rotations. For example, polar vectors change their sign under an inversion, whereas

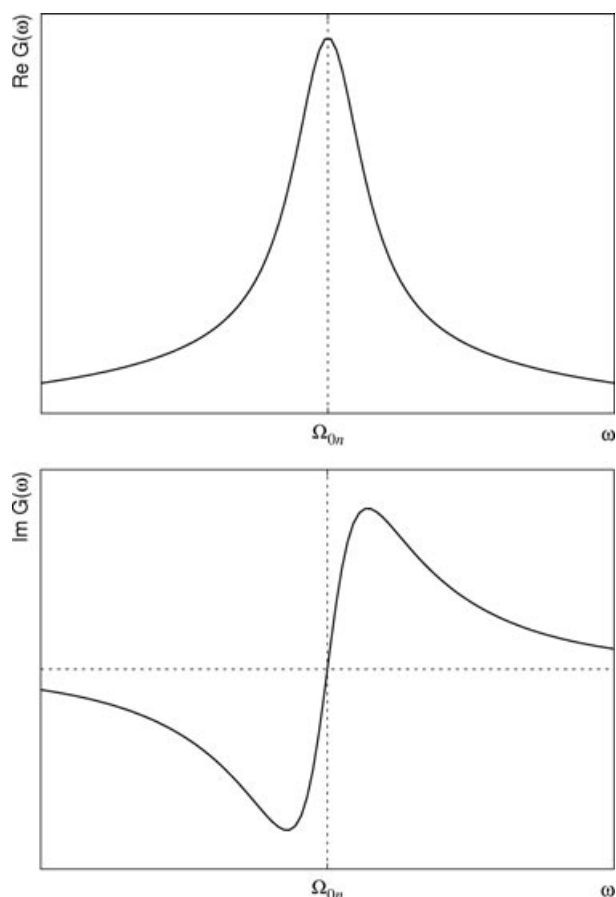


FIGURE 3 | Qualitative behavior of real and imaginary part of $G(\omega)$ close to an excitation energy Ω_{0n} .

axial vectors are invariant. The presence of an improper rotation is thus equivalent to the molecule being achiral.²⁸

As enantiomers behave as mirror images, their rotatory strengths must differ by a sign due to the different transformation properties of $\boldsymbol{\mu}_{0n}$ and \mathbf{m}_{0n} under a reflection. It follows that the ECD and ORD spectra of enantiomers differ in their sign. Thus, ECD and ORD spectra may be used to determine the AC.

Gauge Invariance

The electric transition dipole moment may be evaluated in different gauges.¹⁸ Common choices are the dipole–length gauge,

$$\boldsymbol{\mu}_{0n}^{(l)} = -\langle \Psi_n | \hat{\mathbf{r}} | \Psi_0 \rangle, \quad (16)$$

and the dipole–velocity gauge,

$$\boldsymbol{\mu}_{0n}^{(v)} = -\frac{1}{i\Omega_{0n}} \langle \Psi_n | \hat{\mathbf{p}} | \Psi_0 \rangle, \quad (17)$$

where $\hat{\mathbf{p}}$ denotes the linear momentum operator. This leads to the length and velocity forms of the rotatory

strength:

$$R_{0n}^{(l)} = \text{Im}[\boldsymbol{\mu}_{0n}^{(l)} \cdot \mathbf{m}_{0n}], \quad (18)$$

$$R_{0n}^{(v)} = \text{Im}[\boldsymbol{\mu}_{0n}^{(v)} \cdot \mathbf{m}_{0n}]. \quad (19)$$

Finite basis set approximations to $R_{0n}^{(l)}$ and $R_{0n}^{(v)}$ generally differ; the relative difference can be used as an indicator of basis set quality. Rotatory strengths computed in the dipole–length gauge tend to converge faster with basis set size than those computed in the dipole–velocity gauge. $R_{0n}^{(l)}$ and $R_{0n}^{(v)}$ will differ even in the basis-set limit if approximate response theories such as the Tamm–Dancoff²⁹ approximation are used that do not preserve gauge invariance.

The magnetic transition dipole moment is *not* invariant under a change of the gauge origin \mathbf{R} ,

$$\begin{aligned} \mathbf{m}_{0n}(\mathbf{R}) &= -\frac{1}{2c} \langle \Psi_n | (\hat{\mathbf{r}} - \mathbf{R}) \times \hat{\mathbf{p}} | \Psi_0 \rangle \\ &= -\frac{1}{2c} (\langle \Psi_n | \hat{\mathbf{r}} \times \hat{\mathbf{p}} | \Psi_0 \rangle - \mathbf{R} \times \langle \Psi_n | \hat{\mathbf{p}} | \Psi_0 \rangle) \\ &= \mathbf{m}_{0n}(0) - \frac{i\Omega_{0n}}{2c} \mathbf{R} \times \boldsymbol{\mu}_{0n}^{(v)}. \end{aligned} \quad (20)$$

Because $\boldsymbol{\mu}_{0n}^{(v)} \cdot (\mathbf{R} \times \boldsymbol{\mu}_{0n}^{(v)}) = 0$, the velocity form of the rotatory strength, Eq. (19) is independent of \mathbf{R} , even in a finite basis. However, the length form is not gauge-origin invariant, as long as $|\boldsymbol{\mu}_{0n}^{(v)} - \boldsymbol{\mu}_{0n}^{(l)}| \neq 0$. This spurious gauge-origin dependence can be largely eliminated by using methods and basis sets where $|\boldsymbol{\mu}_{0n}^{(v)} - \boldsymbol{\mu}_{0n}^{(l)}|$ is sufficiently small, or entirely by using gauge-including atomic orbitals (GIAOs, Refs 30–34). As pointed out above, with reasonably polarized basis sets, the length and velocity forms of the electric transition dipole moment should not differ much, and gauge-origin dependence is much less of a concern in ECD and ORD calculations than it is, e.g., for calculations of NMR chemical shieldings.

ELECTRONIC STRUCTURE METHODS FOR ECD

A straightforward approach to the prediction of the electronic CD spectrum, Eq. (9), would be to compute the ground and excited state wavefunctions $|\Psi_0\rangle$, $|\Psi_n\rangle$, and their energies to evaluate the excitation energies and rotatory strengths R_{0n} . In practice, however, almost all modern *ab initio* methods for computing ECD spectra rely on response theory. As opposed to state-based methods such as state-specific complete active space self-consistent field or configuration interaction treatments, which focus on individual excited states, response theory aims at computing all

properties from the response of a reference state to a time-dependent external perturbation. For example, the electric dipole–magnetic dipole polarizability tensor $G_{jk}(\omega)$ is computed from linear response theory as

$$G_{jk}(\omega) = \frac{c}{i\omega} \frac{\partial \mu_j(\mathbf{B}(\omega))}{\partial B_k(\omega)} \Big|_{\mathbf{B}(\omega)=0}, \quad (21)$$

consistent with Eq. (2). This approach has a number of important advantages: (1) The resulting frequency-dependent properties reduce to the correct static limit ($\omega \rightarrow 0$); (2) important constraints, such as the Kramers–Kronig relations linking computed ECD and ORD spectra or sum rules, are automatically satisfied, which is not true for state-specific methods; (3) analytical derivative methods³⁵ may be used to evaluate response properties efficiently; (4) excited-state wavefunctions do not need to be explicitly dealt with.

Different computational strategies are used to evaluate the real and imaginary parts of $G(\omega)$: Excitation energies are obtained from the poles of the frequency-dependent linear response; for example, according to Eq. (4), the excitation energies Ω_{0n} of the states visible in the ECD spectrum are the poles of $G(\omega)$ on the real frequency axis. The rotatory strengths R_{0n} are extracted from the corresponding residues of $G(\omega)$. This is accomplished in practice by computing the Ω_{0n} as eigenvalues of the inverse response function, and construct the residues from the corresponding eigenvectors, as explained below. The real part of $G(\omega)$ at a nonresonant frequency may be computed directly by solving a single linear system of first-order equations²⁴; it is *not* necessary to compute all the excitation energies and rotatory strengths in the SOS expression [Eq. (4)] first.

Time-Dependent Density Functional Theory

Time-dependent density functional theory (TDDFT) is presently the most widely used electronic structure method for ECD calculations. We briefly summarize some key aspects here and refer the reader to more specialized reviews^{36–38} for details.

According to the fundamental Runge–Gross theorem,³⁹ the time-dependent one-particle density $\rho(t, \mathbf{x})$ of a many electron system is uniquely determined by a local multiplicative one-particle potential and vice versa for a fixed initial state; $\mathbf{x} = (\mathbf{r}, \sigma)$ denotes a space-spin coordinate. Runge and Gross introduced a noninteracting system, the so-called time-dependent Kohn–Sham (TDKS) system, which has the same one-particle density as the physical interacting system at all times. The effective one-particle potential

generating the TDKS system is a unique functional of $\rho(t, \mathbf{x})$. Many one-particle response properties can be extracted from the time-dependent density; for example, the time-dependent dipole moment is

$$\boldsymbol{\mu}(t) = - \int d\mathbf{x} \mathbf{r} \rho(t, \mathbf{x}), \quad (22)$$

and thus a perturbation expansion of $\rho(t, \mathbf{x})$ in powers of the external fields yields formally exact polarizabilities.

The exchange–correlation (XC) piece of the TDKS potential is unknown as an explicit density functional. In ECD calculations, the following approximations are used: (1) The XC potential is replaced by its time-independent counterpart, evaluated at the instantaneous density (adiabatic approximation, Ref 40). This corresponds to a neglect of double and higher excitations in the excitation spectrum.⁴¹ (2) The static XC potential is usually approximated using semilocal density functionals, such as generalized gradient approximation^{42–45} (GGA) or hybrid functionals.^{46,47}

As ECD is a mixed electric–magnetic response property, the proper density functional framework to compute ECD intensities is time-dependent current density functional theory.^{48–50} So far, the current dependence of the XC potential has been almost universally neglected. Within time-dependent density functional linear response theory, the electric dipole–magnetic dipole polarizability tensor at complex frequency is obtained as

$$G_{jk}(z) = - \frac{c}{z} \langle \mu^{(j)} | X^{(k)}(z), Y^{(k)}(z) \rangle. \quad (23)$$

In the present notation, a supervector

$$|X, Y\rangle = \begin{pmatrix} X \\ Y \end{pmatrix} \quad (24)$$

consists of two components X and Y , which are elements of the vector spaces $L_{\text{occ}} \times L_{\text{virt}}$ and $L_{\text{virt}} \times L_{\text{occ}}$ spanned by products of occupied (occ) and virtual (virt) ground-state Kohn–Sham (KS) molecular orbitals.⁵¹ $|\mu^{(j)}\rangle = |\mu^{(j)}, \mu^{(j)}\rangle$ contains the matrix elements of the electric dipole moment operator. $|X^{(k)}(z), Y^{(k)}(z)\rangle$ is a solution of the coupled perturbed Kohn–Sham (CPKS) equations at complex frequency,

$$(\Lambda - z\Delta) |X^{(k)}(z), Y^{(k)}(z)\rangle = -|\mathbf{m}^{(k)}\rangle. \quad (25)$$

The 2×2 superoperators

$$\Lambda = \begin{pmatrix} \mathbf{A} & \mathbf{B} \\ \mathbf{B} & \mathbf{A} \end{pmatrix}, \quad \Delta = \begin{pmatrix} \mathbf{1} & \mathbf{0} \\ \mathbf{0} & -\mathbf{1} \end{pmatrix} \quad (26)$$

contain the electric and magnetic orbital rotation Hessians in the adiabatic approximation,

$$(\mathbf{A} + \mathbf{B})_{iajb} = (\varepsilon_a - \varepsilon_i)\delta_{ij}\delta_{ab} + 2(ia|jb) + 2f_{iajb}^{\text{XC}} - c_x[(ib|ja) + (ij|ab)], \quad (27)$$

$$(\mathbf{A} - \mathbf{B})_{iajb} = (\varepsilon_a - \varepsilon_i)\delta_{ij}\delta_{ab} - c_x[(ib|ja) - (ij|ab)], \quad (28)$$

where indices i, j, \dots denote occupied and a, b, \dots virtual canonical KS spin-MOs with eigenvalues ε_i and ε_a , respectively. $(ia|jb)$ is an electron repulsion integral in Mulliken notation, and f_{iajb}^{XC} denotes a matrix element of the static XC kernel,

$$f_{iajb}^{\text{XC}}(x, x') = \frac{\delta^2 E^{\text{XC}}}{\delta\rho(x)\delta\rho(x')}. \quad (29)$$

E^{XC} is the time-independent exchange-correlation energy, e.g., from a semilocal approximation. Becke's hybrid mixing parameter c_x is used to interpolate between nonhybrid TDDFT ($c_x = 0$) and time-dependent Hartree-Fock (TDHF) theory ($c_x = 1$, $E^{\text{XC}} = 0$). The right-hand side $|m^{(k)}\rangle$ contains the k th component of the magnetic dipole moment vector.

If $G(\omega)$ is evaluated at real frequencies ω , the ORD can be computed by solving a single CPKS equation [Refs 20 and 24; Eq. (25)]. For ECD calculations, the imaginary part of G is obtained from the poles and residues of $G(\omega)$ by solving the TDKS eigenvalue problem,^{52,53}

$$(\Lambda - \Omega_{0n}\Delta)|X_n, Y_n\rangle = 0 \quad (30)$$

using the symplectic normalization constraint

$$\langle X_n, Y_n|\Delta|X_n, Y_n\rangle = 1. \quad (31)$$

The eigenvalues Ω_{0n} are the excitation energies, whereas the electric and magnetic transition dipole moments are obtained from the eigenvectors according to

$$\boldsymbol{\mu}_{0n} = \langle X_n, Y_n|\boldsymbol{\mu}\rangle, \quad (32)$$

$$\mathbf{m}_{0n} = \langle X_n, Y_n|\mathbf{m}\rangle, \quad (33)$$

and Eq. (7) yields the rotatory strengths R_{0n} .

The most common XC functionals used for ECD calculations include the Becke-Perdew86 (BP86)^{43,54} and Perdew-Burke-Ernerzhof (PBE)^{45,55} generalized gradient approximation (GGA) functionals along with hybrid functionals such as Becke's three-parameter hybrid (B3LYP)^{43,47,56} and PBE hybrid.⁴⁴⁻⁴⁶ The GGA functionals are susceptible to self-interaction error, which shows up in spurious

charge-transfer intruder states⁵⁷ and unbound Rydberg excitations.^{58,59} Although intensities of individual states are strongly affected by these shortcomings and can be wrong, the overall shape of computed ECD spectra is fairly robust. Range-separated hybrid functionals (CAM-B3LYP),⁶⁰ LC ω -PBE⁶¹⁻⁶⁴ improve long-range CT excitations,⁶⁵ but introduce an additional adjustable parameter. The B2PLYP double-hybrid functional mixes TDDFT and configuration interaction singles with perturbative doubles excitation energies.⁶⁶⁻⁶⁸ Featuring an N^5 scaling of computational cost with the system size N , B2PLYP is significantly more expensive than conventional DFT which scales approximately as N^2 , but B2PLYP does seem to improve excitation energies significantly (see the section *Inherently Chiral Chromophores*). A drawback for ECD spectroscopy is that B2PLYP rotatory strengths do not contain any doubles corrections.⁶⁷

Other Methods

Coupled-cluster response theory is occasionally used to compute ECD^{69,70} and ORD.^{6,71,72} Coupled-cluster singles-doubles (CCSD) calculations exhibit an N^6 scaling of computational cost and are mostly used for benchmarking. The approximate CCSD method CC2 is more economical, particularly in conjunction with resolution-of-identity methods.⁷³⁻⁷⁵ A limitation of coupled cluster response theory for ECD calculations is its lack of gauge invariance.⁷⁶

TDHF calculations of ECD were popular in the 1980s,⁷⁷ but have been superseded by TDDFT. TDDFT using, for example, GGA or hybrid functionals, is considerably more accurate and less susceptible to reference state instabilities than TDHF.^{51,53} Semiempirical methods such as CNDO (Complete Neglect of Differential Overlap)⁷⁸ and related methods can produce accurate valence excitation energies on restricted data sets.⁷⁹

Basis Sets

In most ECD calculations, the molecular orbitals (MOs) φ_p are expanded in a basis of atom-centered functions χ_μ (linear combination of atomic orbitals, LCAO),

$$\varphi_p(\mathbf{r}, \sigma) = \sum_{\mu} C_{\mu p \sigma} \chi_{\mu}(\mathbf{r}). \quad (34)$$

The most common type of basis functions for molecular ECD calculations are Gauss-type orbitals (GTOs), allowing analytical integral evaluation and efficient prescreening in polyatomic systems. Basis sets optimized for ground-state calculations are usually

TABLE 1 | Excitation Energies ΔE (nm) Oscillator Strengths f_{0n} (Length Representation) and Rotatory Strengths R_{0n} (10^{-40} cgs, Length Representation) for the 2^1B State of (M)-hexahelicene. The Structure was Optimized at the HF/SV(P) Level of Theory.⁸⁷ The R_{0n} were Computed Using the PBE Hybrid Functional. SVP, TZP, and QZVP Stand for Polarized Split Valence, Triple- ζ , and Quadruple- ζ Valence Basis Sets.^{88–90} The Suffix D Denotes Diffuse Augmentation⁸⁶

Basis	ΔE	f_{0n}	R_{0n}
SVP	316	0.37	−675
SVPD	320	0.35	−688
TZVP	322	0.35	−700
Sadlej	323	0.35	−701
TZVPD	322	0.35	−701
TZVPPD	323	0.35	−701
QZVPD	323	0.35	−702
Experiment	310	0.4	−400

sufficient for low-lying excitation energies. For a correct description of higher and Rydberg excitations, diffuse functions need to be included in the basis set. Diffuse augmentation is essential for individual transition moments, rotatory strengths, and especially for ORs, which can be qualitatively in error with standard polarized basis sets. The most common diffuse-augmented basis sets include Dunning's hierarchy of augmented correlation-consistent basis sets⁸⁰ and Pople-style basis sets, such as 6-31++G*.^{81–83} Sadlej basis sets^{84,85} are specially designed for polarizability calculations. The recently developed hierarchy of property-optimized Ahlrichs-style basis sets⁸⁶ uses as few diffuse functions as possible and is promising for ECD calculations, particularly in larger systems.

Rotatory strengths are quite sensitive to basis set quality, especially for smaller systems and weak or strongly coupled transitions. Table 1 illustrates the basis set convergence for the first strong band in the ECD spectrum of (M)-hexahelicene.⁸⁷

Although absolute intensities are commonly reproduced within a factor of two by TDDFT³⁸ (see also Table 1), intensities of individual ECD bands relative to each other are considerably more accurate. The use of an appropriate basis set is crucial for the correct prediction of relative intensities and hence for the determination of the AC.

Temperature Effects

To date, most routine applications in theoretical ECD spectroscopy neglect all nuclear motion by using static minimum structures.^{87,91–94} At low temperatures and for rigid molecules, the ECD is dominated by the

chiroptical response of the energetically lowest conformer. In this case, the rotational strengths of only one structure have to be evaluated in order to reasonably reproduce the experimental ECD spectrum or OR. However, the chiroptical response is sensitive to structural changes,⁹⁵ and conformer equilibria lead to important and sometimes qualitative deviations from experiment.^{91,96}

A convenient route for modeling the chiroptical response of moderately flexible molecules consists in computing the ECD spectra of energetically low-lying conformers using quantum chemical methods, followed by Boltzmann averaging.^{97–105} Although this strategy produces satisfactory results in systems with a small number of low-lying conformers separated by high-potential energy barriers, it is not suitable for floppy molecules with soft or strongly anharmonic vibrational modes.

The importance of vibronic effects for OR¹⁰⁴ and ECD^{106,107} has recently been emphasized. General techniques for vibrational averaging are discussed in Refs 108 and 109. Zero-point vibrational corrections can account for up to 20% of the optical rotation.¹⁰⁹ Vibronic model calculations treat the discrete vibrational level structure explicitly.^{106,107,110} However, these models are often based on harmonic normal-mode expansions of the nuclear motion and break down in presence of major changes in structure. Vibrational averaging methods are thus best suited for conformationally restricted molecules. Recently, Dierksen et al.¹¹¹ investigated the origin of ECD of isotopically chiral systems. They concluded that vibronic coupling effects are the main cause for ECD induced by isotopic substitution.

Molecular dynamics (MD) simulations have successfully been used to quantify dynamic and vibronic effects in a classical approximation. These methods involve TDDFT-sampling of the chiroptical response over classical nuclear trajectories. In most cases, these trajectories are obtained using force-field based MD simulations.^{91,112,113} Frelek et al.⁹⁶ used on-the-fly Born–Oppenheimer MD based on full DFT potential energy surfaces in conjunction with TDDFT calculations to sample the chiroptical responses of flexible molecules, see the example in the section *Circular Dichroism of β -lactams*. Although this classical treatment of the nuclei will at best reproduce a correct spectral envelope,⁹⁶ it is the method of choice for systems with significant conformational flexibility that cannot be described in vibronic models. In light of the sometimes complex relation between ECD and conformation, the use of force-field-based classical potential energy surfaces instead of the quantum mechanical ones should be carefully validated.

A simplistic but widely used method to include temperature and solvent effects in ECD spectra qualitatively is empirical line broadening. As established by Mason et al.,¹¹⁴ Gaussians of constant line width centered at the excitation energies and scaled to integrate to the computed rotatory strengths according to Eq. (10) may be used to approximate the ECD spectrum. In this procedure, the Gaussian root mean square width is an empirical parameter which is usually chosen to fit the measured spectrum. For ECD spectra in the near UV and visible region, a typical root mean square width is 0.15eV.

Solvent Effects

ECD and OR depend sensitively on the presence and nature of solvent interactions.^{70,115–117} The change in chiroptical response due to solute–solvent interactions is sometimes drastic and nonintuitive. A well-known example is the sign inversion in the OR of methyloxirane upon changing the solvent from water to benzene.¹¹⁶ Strong solvatochromism in ECD spectra may arise from solvent effects on tautomer equilibria,¹¹⁸ as illustrated in the section *Absolute Configuration and Solvatochromism of [2.2]Paracyclophane Ketimines*. Different strategies exist to include solvent–solute interactions into chiroptical response calculations. Continuum models such as the conductor-like screening model (COSMO)^{119–121} or the polarizable continuum model (PCM)^{122–124} account for electrostatic and polarization effects between a continuous solvent and the molecule.^{125,126} Classical force-field MD simulations constitute a possible route to explicitly account for interactions between molecule and solvent.^{91,117,127} Apart from the high computational cost it might appear most desirable to treat the solute embedded in a large number of solvent molecules within a first-principles quantum mechanical MD approach. This might only be possible with very efficient electronic structure methods such as DFT which on the other hand have deficiencies for non-covalent long-range interactions. Semiempirical models developed for large scale solvent simulations might be a viable alternative for simulating chiroptical properties in the presence of explicit solvent interactions.¹⁹

APPLICATIONS

Inherently Chiral Chromophores

A classical example of inherently chiral chromophores are helicenes. These helical polyacenes exhibit strong ECD in the UV and OR values of 1000 °/(dm(g/cm³)) and more. TDDFT using the BP86 functional and

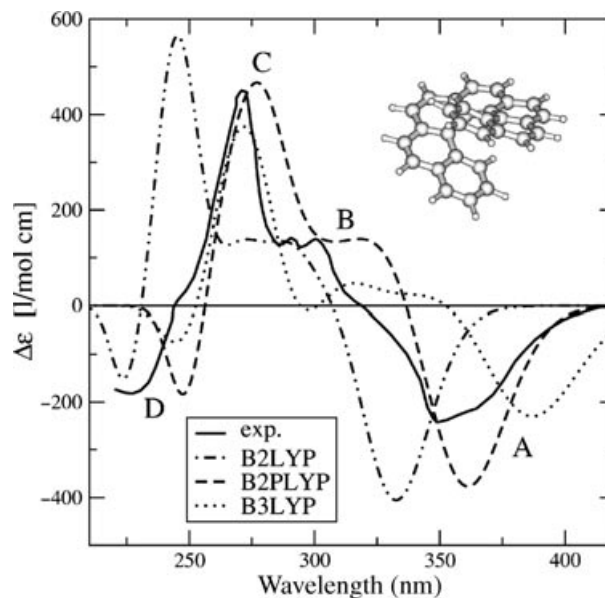


FIGURE 4 | Comparison of TDDFT⁶⁷ and experimental¹²⁸ circular dichroism spectra for (M)-[7]helicene with the three different density functionals B2LYP, B2PLYP,⁶⁶ and B3LYP along with the TZVP basis set. (Reprinted with permission from Ref 67. Copyright 2007 American Institute of Physics.)

polarized split-valence basis sets is accurate enough to determine the AC of helicenes, and can even be used to identify substituted helicenes by their ECD signature.⁸⁷ Figure 4 shows a comparison of three hybrid functionals for [7]-helicene. The B2PLYP double hybrid outperforms the two other functionals by placing bands A and C in the right position, but has deficiencies at higher energies.⁶⁷

Most higher fullerenes are inherently chiral. It is very difficult to isolate and separate fullerene enantiomers, and ECD spectroscopy is often the only reliable option to determine their AC. Resolution of the enantiomers of *D*₂-C₈₄ was first achieved by Diederich et al.¹²⁹ in 1999, but existing semiempirical CNDO/S ECD data¹³⁰ were not accurate enough to pin down the AC. On the other hand, TDDFT using the BP86 functional reproduces the main features of the experimental spectrum¹³¹ (see Figure 5), thus allowing a definite assignment of the AC. The computed absolute ECD intensities of *D*₂-C₈₄ are substantially larger than the measured ones, for reasons not well understood.¹³¹

Absolute Configuration of Iso-schizogaline and Iso-schizogamine

A paper by Stephens et al. on the two natural products iso-schizogaline and iso-schizogamine¹³³ (Figure 6) illustrates the scope and the limitations of ECD spectroscopy in determining the AC of organic molecules

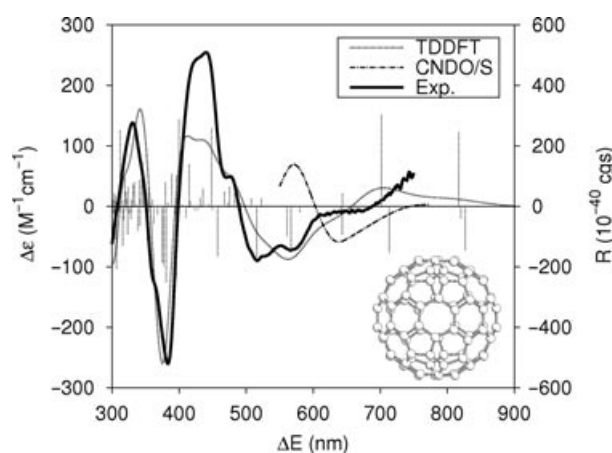


FIGURE 5 | Experimental ECD spectrum¹²⁹ of D_2 - C_{84} compared to simulations using a semiempirical method¹³⁰ and TDDFT¹³¹ (BP86/aug-SVP). The absolute configuration of the fullerene is $^f A$ in the old¹²⁹ and C in the new IUPAC¹³² nomenclature. ϵ denotes the molar decadic absorption coefficient, R the rotatory strength. Calculated $\Delta\epsilon$ values from TDDFT were scaled by 1/14 to match the experimental intensities. (Data reprinted with permission from Ref 131. Copyright 2002 American Chemical Society. CNDO/S data reprinted with permission from Ref 130. Copyright 1997 Elsevier.)



FIGURE 6 | Iso-schizogamine and iso-schizogaline.

with several stereocenters. Iso-schizogamine and iso-schizogaline contain four asymmetric carbon atoms, corresponding to eight enantiomer pairs. To fully resolve the AC of all four stereocenters, the authors compare simulated and experimental chiroptical data from three different methods: ECD, OR, and vibrational CD. Rotatory strengths, optical rotations, and vibrational spectra³¹ of the low-lying conformers were obtained using B3LYP and gauge-including atomic orbitals.³² The three methods yield consistent results and predict the AC of natural iso-schizogaline and iso-schizogamine to be (2R,7R,20S,21S). ECD spectroscopy alone is not sufficient for a reliable AC assignment here, due to strongly overlapping bands in the experimental ECD spectrum.

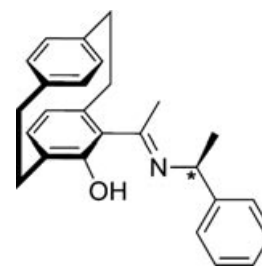


FIGURE 7 | [2.2]paracyclophane-ketimine derivative featuring planar and central chirality.

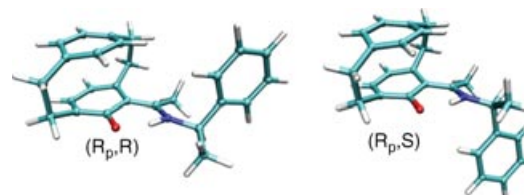


FIGURE 8 | Structures of the low-energy conformers of the (R_p,R) and (R_p,S) diastereomers. (Reprinted with permission from Ref 118. Copyright 2009 American Chemical Society.)

Absolute Configuration and Solvatochromism of [2.2]Paracyclophane Ketimines

ECD spectra and the AC of moderately flexible [2.2]paracyclophanes were recently investigated by Warnke et al.¹¹⁸ [2.2]paracyclophanes are highly efficient chiral ligands used in 1,2-additions and conjugate 1,4-additions of organozinc compounds to aldehydes and ketones. They feature planar chirality in the paracyclophane moiety as well as an asymmetric carbon atom in the ketimine side chain (see Figure 7).

The authors employ ECD and OR as obtained from TDDFT calculations and compare them to experimental data. Geometry optimizations including COSMO for the treatment of solvent effects reveal that diastereomers adopt different conformations (see Figure 8), causing differences in their ECD spectra: The sign of the lowest-energy ECD band at 361 nm is determined by the AC of the planar chiral paracyclophane moiety. This is not surprising as the lowest excitation is characterized by a $\pi \rightarrow \pi^*$ transition from the highest occupied to the lowest unoccupied molecular orbital, which is delocalized over the parts of the paracyclophane moiety. On the other hand, the intensity of the lowest CD band is sensitive to the relative orientation between the paracyclophane and the phenyl group in the ketimine side chain. This orientation is different for diastereomers (see Figure 8): The AC of the asymmetric side-chain carbon is determined by means of the intensity of the ECD band

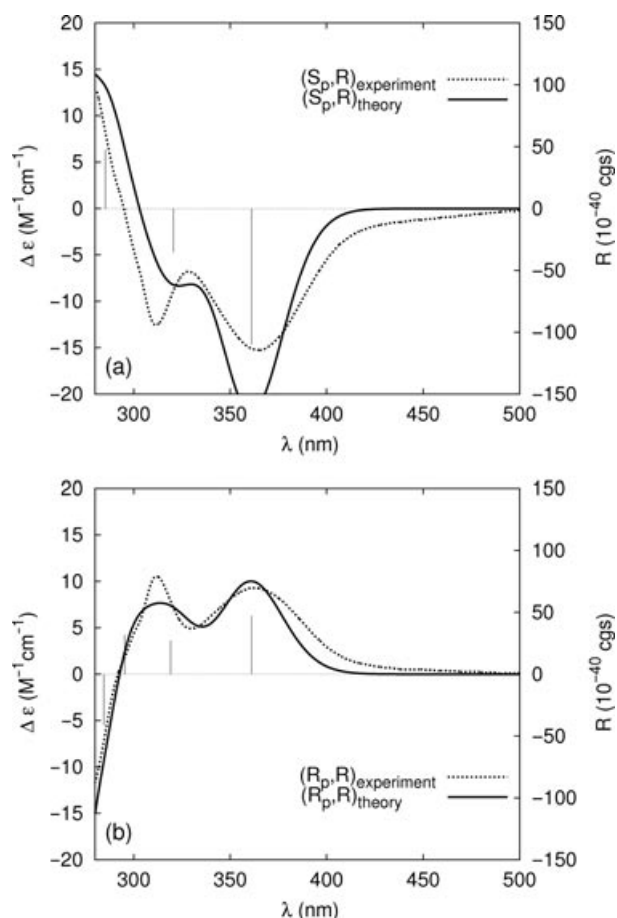


FIGURE 9 | Experimental electronic circular dichroism (ECD) of a pair of diastereomers recorded in toluene is compared to corresponding theoretical spectra from time-dependent density functional theory (TDDFT) response calculations PBE hybrid functional/split-valence plus polarization basis set. Solvent effects are included using COSMO (see the section *Solvent Effects*). Calculated spectra were scaled with a factor 0.5. Root mean square linewidth for Gaussian broadening is 0.15eV (see section *Temperature Effects*). The predicted difference in the absolute intensities of the lowest-energy band is present in the measured spectra. (Reprinted with permission from Ref 118. Copyright 2009 American Chemical Society.)

at 361 nm. Comparison of experimental and theoretical ECD (Figure 9) confirms the presence of the predicted change in sign and difference in intensities in the experimental data and allows for reliable AC determination.

The inclusion of solvent effects is vital for this system: Strong solvatochromism in the experimental spectrum (Figure 10) is caused by the influence of the solvent polarity on a tautomer equilibrium between an aromatic *ortho*-hydroquinone-imine form and an *ortho*-quinone enamine form of the molecule (Figure 11): Polar solvents favor the quinoidal, more

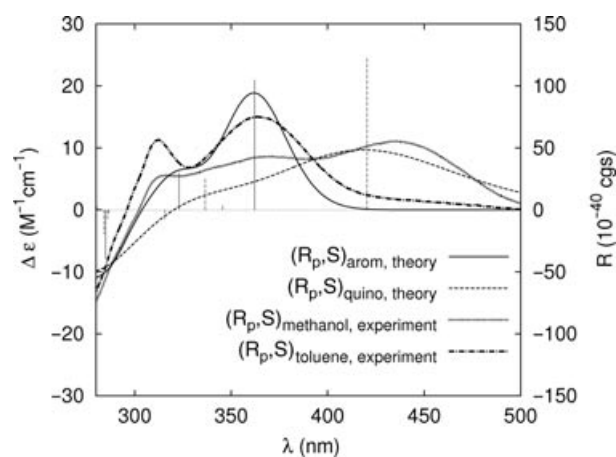


FIGURE 10 | Computed and measured electronic circular dichroism (ECD) of the tautomeric forms (R_p,S)-*arom* and (R_p,S)-*quino* of the studied [2.2]paracyclophane-ketimine derivative (Figure 7). The less polar solvent favors the less polar *ortho*-hydroquinone-imine whereas the more polar solvent promotes the *ortho*-quinone-enamine tautomer. Computed spectra were obtained from time-dependent density functional theory (TDDFT) (PBE hybrid/SVP) response calculations. Root mean square linewidths are 0.15eV for the aromatic tautomer and 0.30eV for the quinoidal tautomer (see the section *Temperature Effects*). Theoretical spectra are scaled by a factor 0.45. (Reprinted with permission from Ref 118. Copyright 2009 American Chemical Society.)

polar tautomer and unpolar solvents cause the aromatic, less polar tautomer to be more stable. The two tautomeric forms are spectroscopically distinct species. The quinoidal, nonaromatic form features substantially red-shifted excitation energies. To reproduce spectra recorded in solvents of intermediate polarity, COSMO calculations were used to determine the solvent dependent Boltzmann factors for a weighted average of the theoretical spectra of both tautomers (see Figure 12).

Circular Dichroism of β -lactams

The experimentally measured ECD is dominated by the chiroptical response of the lowest conformer only for rigid molecules. Thermal effects can exceed inaccuracies inherent to TDDFT and in some cases even lead to qualitatively different spectra. A treatment of thermal effects becomes necessary for flexible molecules. In a study on models for conformationally flexible β -lactam antibiotics, Frelek et al.⁹⁶ explored a new strategy to systematically address the effects of nuclear motion: they combined TDDFT calculations with full quantum-mechanical Born–Oppenheimer MD using DFT ground-state potential energy surfaces. This computationally demanding approach involves sampling over tens of thousands of time-steps

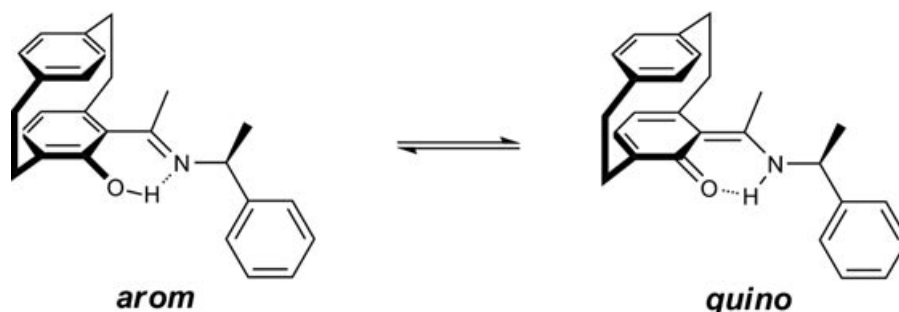


FIGURE 11 | Tautomeric equilibrium explaining the observed solvatochromism. **arom** is the *ortho*-hydroquinone-imine form and **quino** is the *ortho*-quinone-enamine form.

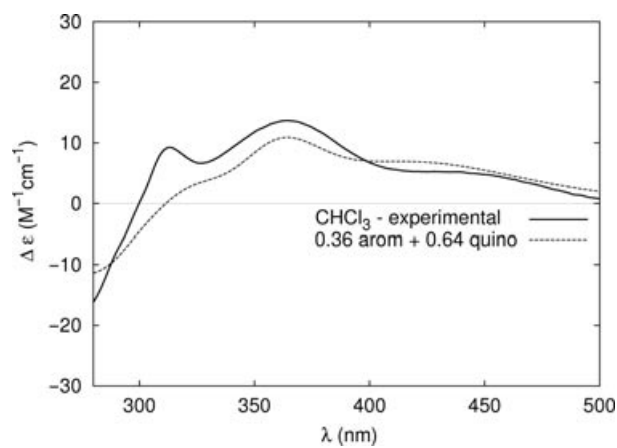


FIGURE 12 | Boltzmann-weighted superposition of the computed *ortho*-quinone enamine and *ortho*-hydroquinone-imine electronic circular dichroism (ECD) spectra versus ECD spectrum of the (*R_p*,*S*) diastereomer recorded in chloroform. Computed circular dichroism spectra from time-dependent density functional theory (TDDFT) (PBE hybrid/SVP) calculations, scaled by a factor 0.5. Conformer energies for Boltzmann-factors were computed including solvent effects through COSMO (see section *Solvent Effects*). For details see Ref 118. (Reprinted with permission from Ref 118. Copyright 2009 American Chemical Society.)

and has become possible with the availability of highly efficient DFT and TDDFT implementations.¹³⁴

The carbacepham depicted in Figure 13 is one of the investigated model systems. Figure 14 compares the corresponding experimental ECD to the simulated ECD of the lowest conformer at 0 K as well as to the ECD curve resulting from the MD simulation. The qualitative difference between the two theoretical curves is attributed to a complex relation between ECD and the structure of individual conformers; different conformers of one enantiomer can have radically different ECD spectra. The reasonable agreement between experiment and MD result allows for AC assignment and emphasizes the importance of incorporating temperature effects. In this case, vibra-

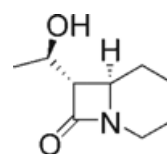


FIGURE 13 | The investigated (6*R*,7*S*)-7-((1*R*)-1-hydroxyethyl)-8-oxo-1-aza-bicyclo[4.2.0]octane.

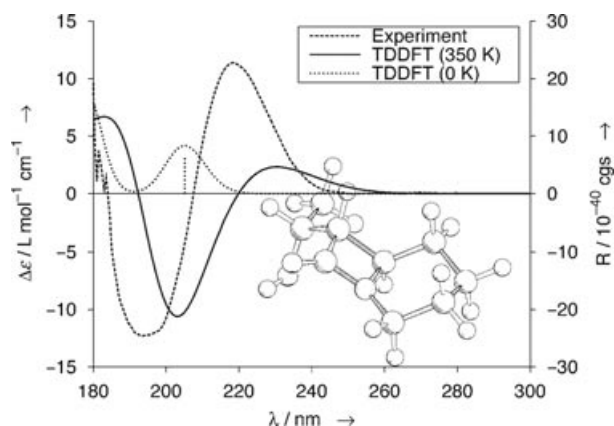


FIGURE 14 | Computed structure of the cepham analog (see Figure 13) and its simulated electronic circular dichroism (ECD) spectrum at 0 K and 350 K compared to experiment. The 0 K curve corresponds to the conformer shown, whereas the 350 K curve is the result of MD simulation. ϵ is the molar decadic absorption coefficient, λ the wavelength, and R the computed rotatory strength. The experimental spectrum was recorded in acetonitrile at room temperature. See Ref 96 for details. (Data reprinted with permission from Ref 96. Copyright 2007 Wiley-VCH Verlag GmbH & Co.)

tional averaging is not a suitable alternative because large-amplitude motions and conformational dynamics are present.

In combination with MD-based ECD simulations, the temperature-dependence of experimental ECD spectra can provide detailed insight in conformational dynamics.¹⁰⁵ The authors found that a previously developed helicity rule¹³⁵ for the simple AC

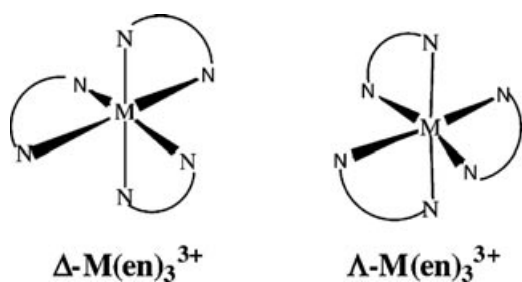


FIGURE 15 | Δ - and Λ -configuration of $[\text{Co}(\text{en})_3]^{3+}$.

assignment in cephams only holds for conformationally averaged spectra.

Stereochemistry of Transition Metal Complexes

DFT is the workhorse of computational transition metal (TM) chemistry, although inaccuracies are substantially larger than in main group chemistry.¹³⁶ ECD spectra of TM complexes are complicated by $d \rightarrow d$ transitions and metal-to-ligand CT transitions.

Wang et al.¹³⁷ pioneered the theoretical ECD spectroscopy of octahedral *tris*-(didentate) complexes using TDDFT almost 10 years ago. Jorge et al.¹³⁸ explored the possibility of using TDDFT to elucidate the role of configurational and conformational effects on ECD spectra of *tris*-diamine Co(III) and Rh(III) complexes. Octahedral *tris*-bidentate TM complexes occur in two enantiomeric configurations. The configuration is denoted Δ if the chelating ligands are arranged around the TM in form of a right-handed helix, and Λ for a left-handed helix (see Figure 15). When coordinated to the central TM, each ligand chain can adopt two different conformations, δ or λ . The configuration-conformation combinations Δ -($\lambda\lambda\lambda$) and Λ -($\delta\delta\delta$) are called *lel*₃ and the forms Δ -($\delta\delta\delta$) and Λ -($\lambda\lambda\lambda$) are called *ob*₃. Further complications arise from polar and azimuthal distortions¹³⁹ from the ideal octahedral coordination geometry.

The first step in studying the OA is conformational analysis. In agreement with force-field based estimations, DFT calculations including solvent effects (COSMO) predict the *lel*₃-forms of the $[\text{Co}(\text{en})_3]^{3+}$ cation to be slightly more stable than the corresponding *ob*₃ form. Thus, in the case of ethylene-diamine ligands, the preferred ligand conformation is linked to the AC of the TM complex. However, the preferred conformation adopted by the chiral ligand (1,2)-propyl-diamine (*pn*) is no longer controlled by the AC of the complex, but by the AC of the ligand

itself: (*S*)-*pn* and (*R*)-*pn* ligands preferably adopt δ and λ conformation, respectively. This situation allows a systematic study of the influence of ligand conformation on the ECD spectra: By successively replacing, e.g., the *en* ligands with (*S*)-*pn* in a Δ -($\lambda\lambda\lambda$) complex, it is possible to gradually move from a *lel*₃ to an *ob*₃ complex. The authors compare their theoretical results to the available experimental ECD spectra.^{140, 141} They also compare the theoretical spectrum of the energetically unfavored *ob*₃ form to the experimental and theoretical ECD of the *lel*₃ form. The energetically low-lying ECD bands are dominated by $d \rightarrow d$ type transitions, whereas ECD transitions from the central metal ion to the ligands are present in the high-energy region. Based on their TDDFT results, the authors discuss a simplified model¹⁴² for rationalizing qualitative trends in the influence of ligand conformation on the rotatory strengths of $d \rightarrow d$ and CT transitions.

CONCLUSIONS

Theory-aided ECD spectroscopy is an inexpensive and fast tool for determining the AC of a wide range of rigid systems. For a reliable assignment of the AC, ECD spectra should be computed and measured over a range of several hundred nm and should show two or more distinct features. If possible, assignments by ECD should be complemented by at least one other chiroptical measurement, including OR, vibrational CD, or Raman optical activity,^{9, 10} especially if several chirality elements are present. Moderately flexible systems can be treated by Boltzmann-averaging the computed ECD spectra of the energetically lowest conformers. This requires careful conformational analysis, e.g., using force field molecular mechanics.

Although ECD calculations of simple rigid systems can routinely be performed by nonspecialists, the simulation of detailed vibronic structure and the treatment of highly flexible molecules remains difficult and computationally demanding. Higher accuracy is often required for distinguishing diastereomers or for ECD-based determinations of structural parameters such as dihedral angles. TDDFT is the method of first choice for ECD calculations, but in its present form is not universally accurate, with major limitations including charge transfer and Rydberg excitations, as well as double and higher excitations. Despite the remarkable progress that theoretical ECD spectroscopy has seen in the past decade, there is ample room for further developments.

ACKNOWLEDGMENTS

We acknowledge support by the NSF Center for Chemical Innovation 'Chemistry at the Space-Time Limit' CaSTL, Grant No. CHE-0802913.

REFERENCES

1. Berova N, Nakanishi K, Woody RW. *Circular Dichroism: Principles and Applications*. New York: Wiley-VCH; 2000.
2. Carnell M, Grimme S, Peyrerimhoff S. Theoretical study of the circular dichroism and VUV spectra of trans-2,3-dimethyloxirane. *Chem Phys* 1994, 179:385–394.
3. Autschbach J, Ziegler T, van Gisbergen SJA, Baerends EJ. Chiroptical properties from time-dependent density functional theory. I. Circular dichroism spectra of organic molecules. *J Chem Phys* 2002, 116:6930–6940.
4. Bijvoet JM, Peerdeman AF, van Bommel AJ. Determination of the absolute configuration of optically active compounds by means of X-rays. *Nature* 1951, 168:271–272.
5. Flack H, Bernardinelli G. The use of X-ray crystallography to determine absolute configuration. *Chirality* 2008, 20:681–690.
6. Crawford TD, Stephens PJ. Comparison of time-dependent density-functional theory and coupled cluster theory for the calculation of the optical rotations of chiral molecules. *J Chem Phys A* 2008, 112:1339–1345.
7. Crawford TD. Ab initio calculation of molecular chiroptical properties. *Theor Chem Acc* 2006, 115:227–245.
8. Polavarapu PL. Optical rotation: recent advances in determining the absolute configuration. *Chirality* 2002, 14:768–781.
9. Polavarapu PL. Renaissance in chiroptical spectroscopic methods for molecular structure determination. *Chem Rec* 2007, 7:125–136.
10. Polavarapu PL. Why is it important to simultaneously use more than one chiroptical spectroscopic method for determining the structures of chiral molecules? *Chirality* 2008, 20:664–672.
11. Fasman GD. *Circular Dichroism and the Conformational Analysis of Biomolecules*. New York: Plenum Press; 1996.
12. Manavalan P, Johnson WC. Protein secondary structure from circular dichroism spectra. *J Biosci* 1985, 8:141–149.
13. Sreerama N, Venyaminov SY, Woody RW. Estimation of protein secondary structure from circular dichroism spectra: inclusion of denatured proteins with native proteins in the analysis. *Anal Biochem* 2000, 287:243–251.
14. Barron LD. *Molecular Light Scattering and Optical Activity*. New York: Cambridge University Press; 2004.
15. Charney E. *The Molecular Basis of Optical Activity*. New York: John Wiley & Sons; 1979.
16. Lightner DA, Gurst JE. *Organic Conformational Analysis and Stereochemistry from Circular Dichroism Spectroscopy*. New York: Wiley-VCH; 2000.
17. Caldwell DJ, Eyring H. *The Theory of Optical Activity*. New York: John Wiley & Sons; 1971.
18. Hansen AE, Bouman TD. Natural chiroptical spectroscopy: theory and computations. *Adv Chem Phys* 1980, 44:545–644.
19. Autschbach J. Computing chiroptical properties with first-principles theoretical methods: background and illustrative examples. *Chirality* 2009, 21:E116–E152.
20. Krykunov M, Autschbach J. Calculation of origin-independent optical rotation tensor components in approximate time-dependent density functional theory. *J Chem Phys* 2006, 125:034102 (10 pages).
21. Rosenfeld L. Quantenmechanische Theorie der natürlichen optischen Aktivität von Flüssigkeiten und Gasen. *Z Phys* 1929, 52:161–174.
22. Jackson JD. *Classical Electrodynamics*. New York: John Wiley & Sons; 1962.
23. Condon EU. Theories of optical rotatory power. *Rev Mod Phys* 1937, 9:432–457.
24. Grimme S, Furche F, Ahlrichs R. An improved method for density functional calculations of the frequency-dependent optical rotation. *Chem Phys Lett* 2002, 361:321–328.
25. Kronig RDL. On the theory of dispersion of X-rays. *J Opt Soc Am* 1926, 12:547–556.
26. Moffitt W, Moscovitz A. Optical activity in absorbing media. *J Chem Phys* 1959, 30:648–660.
27. Moscovitz A. Some applications of the Kronig-Kramers theorem to optical activity. *Tetrahedron* 1961, 13:48–56.
28. Cotton FA F. *Chemical Applications of Group Theory*. 3rd ed. New York: Wiley; 1990.

29. Hirata S, Head-Gordon M. Time-dependent density functional theory within the Tamm–Dancoff approximation. *Chem Phys Lett* 1999, 314:291–299.
30. London F. Quantum theory of interatomic currents in aromatic compounds. Théorie quantique des courants interatomiques dans les combinaisons aromatiques. *J Phys Rad* 1937, 8:397–409.
31. Stephens PJ. Theory of vibrational circular dichroism. *J Phys Chem* 1985, 89:748–752.
32. Cheeseman JR, Frisch MJ, Devlin FJ, Stephens PJ. Ab initio calculation of atomic axial tensors and vibrational rotational strengths using density functional theory. *Chem Phys Lett* 1996, 252:211–220.
33. Cheeseman JR, Frisch MJ, Devlin FJ, Stephens PJ. Hartree–Fock and density functional theory ab initio calculation of optical rotation using GIAOs: basis set dependence. *J Chem Phys A* 2000, 104:1039–1046.
34. Jusélius J, Sundholm D, Gauss J. Calculation of current densities using gauge-including atomic orbitals. *J Chem Phys* 2004, 121:3952–3963.
35. Pulay P. Analytical derivative methods in quantum chemistry. In: *Advance in Chemical Physics*. New York: John Wiley & Sons, Inc.; 1987, 241–286.
36. Rappoport D, Furche F. Density functional methods for excited states: equilibrium structure and electronic spectra. In: *Computational Photochemistry*. Amsterdam: Elsevier; 2005.
37. Marques MAL, Ullrich CA, Nogueira F, Rubio A, Burke K, Gross EKV. *Time-Dependent Density Functional Theory*. Berlin: Springer; 2006.
38. Elliott P, Furche F, Burke K. Excited states from time-dependent density functional theory. In: *Reviews in Computational Chemistry*. Hoboken, NJ: John Wiley & Sons; 2009, 91–165.
39. Runge E, Gross EKV. Density-functional theory for time-dependent systems. *Phys Rev Lett* 1984, 52:997–1000.
40. Gross EKV, Kohn W. Time-dependent density-functional theory. *Adv Quant Chem* 1990, 21:255–291.
41. Maitra NT, Zhang F, Cave RJ, Burke K. Double excitations within time-dependent density functional theory linear response. *J Chem Phys* 2004, 120:5932–5937.
42. Langreth D. Beyond the local-density approximation in calculations of ground-state electronic properties. *Phys Rev B* 1983, 28:1809–1834.
43. Becke AD. Density-functional exchange-energy approximation with correct asymptotic behavior. *Phys Rev A* 1988, 38:3098–3100.
44. Perdew J. Atoms, molecules, solids, and surfaces: applications of the generalized gradient approximation for exchange and correlation. *Phys Rev B* 1992, 46:6671–6687.
45. Perdew J. Generalized gradient approximation made simple. *Phys Rev Lett* 1996, 77:3865–3868.
46. Perdew JP, Ernzerhof M, Burke K. Rationale for mixing exact exchange with density functional approximations. *J Chem Phys* 1996, 105:9982–9985.
47. Becke AD. Density-functional thermochemistry. III. The role of exact exchange. *J Chem Phys* 1993, 98:5648–5652.
48. Ullrich CA, Vignale G. Time-dependent current-density-functional theory for the linear response of weakly disordered systems. *Phys Rev B* 2002, 65:245102 (19 pages).
49. Vignale G, Kohn W. Current-dependent exchange-correlation potential for dynamical linear response theory. *Phys Rev Lett* 1996, 77:2037–2040.
50. van Faassen M, de Boeij PL. Excitation energies for a benchmark set of molecules obtained within time-dependent current-density functional theory using the Vignale–Kohn functional. *J Chem Phys* 2004, 120:8353–8363.
51. Furche F. On the density matrix based approach to time-dependent density functional response theory. *J Chem Phys* 2001, 114:5982–5992.
52. Casida ME. *Recent Developments and Applications in Density-Functional Theory*. Amsterdam: Elsevier; 1996.
53. Bauernschmitt R, Ahlrichs R. Treatment of electronic excitations within the adiabatic approximation of time dependent density functional theory. *Chem Phys Lett* 1996, 256:454–464.
54. Perdew J. Density-functional approximation for the correlation energy of the inhomogeneous electron gas. *Phys Rev B* 1986, 33:8822–8824.
55. Perdew J. Accurate and simple analytic representation of the electron-gas correlation energy. *Phys Rev B* 1992, 45:13244–13249.
56. Lee C, Yang W, Parr RG. Development of the Colle–Salvetti correlation-energy formula into a functional of the electron density. *Phys Rev B* 1988, 37:785–789.
57. Dreuw A, Weisman JL, Head-Gordon M. Long-range charge-transfer excited states in time-dependent density functional theory require non-local exchange. *J Chem Phys* 2003, 119:2943–2946.
58. Casida ME, Jamorski C, Casida KC, Salahub DR. Molecular excitation energies to high-lying bound states from time-dependent density-functional response theory: characterization and correction of the time-dependent local density approximation ionization threshold. *J Chem Phys* 1998, 108:4439–4449.
59. Casida ME, Salahub DR. Asymptotic correction approach to improving approximate exchange-correlation potentials: time-dependent density-functional theory calculations of molecular excitation spectra. *J Chem Phys* 2000, 113:8918.

60. Yanai T. A new hybrid exchange-correlation functional using the Coulomb-attenuating method (CAM-B3LYP). *Chem Phys Lett* 2004, 393:51–57.
61. Tawada Y, Tsuneda T, Yanagisawa S, Yanai T, Hirao K. A long-range-corrected time-dependent density functional theory. *J Chem Phys* 2004, 120:8425–8433.
62. Vydrov OA, Scuseria GE. Assessment of a long-range corrected hybrid functional. *J Chem Phys* 2006, 125:234109 (9 pages).
63. Vydrov OA, Heyd J, Krukau AV, Scuseria GE. Importance of short-range versus long-range Hartree–Fock exchange for the performance of hybrid density functionals. *J Chem Phys* 2006, 125:074106 (9 pages).
64. Vydrov OA, Scuseria GE, Perdew JP. Tests of functionals for systems with fractional electron number. *J Chem Phys* 2007, 126:154109 (9 pages).
65. Peach MJG, Benfield P, Helgaker T, Tozer DJ. Excitation energies in density functional theory: an evaluation and a diagnostic test. *J Chem Phys* 2008, 128:044118 (8 pages).
66. Grimme S. Semiempirical hybrid density functional with perturbative second-order correlation. *J Chem Phys* 2006, 124:034108 (16 pages).
67. Grimme S, Neese F. Double-hybrid density functional theory for excited electronic states of molecules. *J Chem Phys* 2007, 127:154116 (18 pages).
68. Head-Gordon M, Rico RJ, Oumi M, Lee TJ. A doubles correction to electronic excited states from configuration interaction in the space of single substitutions. *Chem Phys Lett* 1994, 219:21–29.
69. Pedersen TB, Koch H, Ruud K. Coupled cluster response calculation of natural chiroptical spectra. *J Chem Phys* 1999, 110:2883.
70. Kongsted J, Pedersen TB, Osted A, Hansen AE, Mikkelsen KV, Christiansen O. Solvent effects on rotatory strength tensors. 1. Theory and application of the combined coupled cluster/dielectric continuum model. *J Chem Phys A* 2004, 108:3632–3641.
71. Crawford TD, Allen W. Optical activity in conformationally flexible molecules: a theoretical study of large-amplitude vibrational averaging in (R)-3-chloro-1-butene. *Mol Phys* 2009, 107:1041–1057.
72. Ruud K, Helgaker T. Optical rotation studied by density-functional and coupled-cluster methods. *Chem Phys Lett* 2002, 352:533–539.
73. Hättig C, Weigend F. CC2 excitation energy calculations on large molecules using the resolution of the identity approximation. *J Chem Phys* 2000, 113:5154–5161.
74. Hättig C, Kohn A. Transition moments and excited-state first-order properties in the coupled-cluster model CC2 using the resolution-of-the-identity approximation. *J Chem Phys* 2002, 117:6939–6951.
75. Hättig C, Hald K. Implementation of RI-CC2 triplet excitation energies with an application to trans-azobenzene. *Phys Chem Chem Phys* 2002, 4:2111–2118.
76. Pedersen TB, Fernández B, Koch H. Gauge invariant coupled cluster response theory using optimized nonorthogonal orbitals. *J Chem Phys* 2001, 114:6983–6993.
77. Hansen AE, Bouman TD. Optical activity of monoolefins: RPA calculations and extraction of the mechanisms in Kirkwood's theory. Application to (-)-trans-cyclooctene and 3(3R)-3-methylcyclopentene. *J Am Chem Soc* 1985, 107:4828–4839.
78. Pople JA, Santry DP, Segal GA. Approximate self-consistent molecular orbital theory. I. Invariant procedures. *J Chem Phys* 1965, 43:S129–S135.
79. Bringmann G. Circular dichroism of naphthyltetrahydroisoquinoline alkaloids: calculation of CD spectra by semiempirical methods. *Tetrahedron* 1993, 49:3305–3312.
80. Peterson KA, Dunning TH. Accurate correlation consistent basis sets for molecular core–valence correlation effects: the second row atoms Al–Ar, and the first row atoms B–Ne revisited. *J Chem Phys* 2002, 117:10548–10560.
81. Hehre WJ. Self-consistent molecular orbital methods. XII. Further extensions of gaussian-type basis sets for use in molecular orbital studies of organic molecules. *J Chem Phys* 1972, 56:2257–2261.
82. Dill JD. Self-consistent molecular orbital methods. XV. Extended Gaussian-type basis sets for lithium, beryllium, and boron. *J Chem Phys* 1975, 62:2921–2923.
83. Francl MM. Self-consistent molecular orbital methods. XXIII. A polarization-type basis set for second-row elements. *J Chem Phys* 1982, 77:3654–3665.
84. Sadlej AJ. Molecular electric polarizabilities. Electronic-field-variant (EFV) Gaussian basis set for polarizability calculations. *Chem Phys Lett* 1977, 47:50–54.
85. Sadlej AJ. Medium-size polarized basis sets for high-level-correlated calculations of molecular electric properties. *Theor Chim Acta* 1991, 81:45–63.
86. Rappoport D, Furche F. Property-optimized Gaussian basis sets for molecular response calculations. *J Chem Phys* 2010, 133:134105 (10 pages).
87. Furche F, Ahlrichs R, Wachsmann C, Weber E, Sobanski A, Vogtle F, Grimme S. Circular dichroism of helicenes investigated by time-dependent density functional theory. *J Am Chem Soc* 2000, 122:1717–1724.
88. Schäfer A, Horn H, Ahlrichs R. Fully optimized contracted Gaussian-basis sets for atoms Li to Kr. *J Chem Phys* 1992, 97:2571–2577.
89. Schäfer A, Huber C, Ahlrichs R. Fully optimized contracted Gaussian-basis sets of triple zeta valence quality for atoms Li to Kr. *J Chem Phys* 1994, 100:5829–5835.

90. Weigend F, Ahlrichs R. Balanced basis sets of split valence, triple zeta valence and quadruple zeta valence quality for H to Rn: design and assessment of accuracy. *Phys Chem Chem Phys* 2005, 7:3297–3305.
91. Kundrat MD, Autschbach J. Modeling of the chiroptical response of chiral amino acids in solution using explicit solvation and molecular dynamics. *J Chem Theory Comput* 2009, 5:1051–1060.
92. Autschbach J, Patchkovskii S, Ziegler T, van Gisbergen SJA, Jan Baerends E. Chiroptical properties from time-dependent density functional theory. II. Optical rotations of small to medium sized organic molecules. *J Chem Phys* 2002, 117:581–592.
93. Diedrich C, Grimme S. Systematic investigation of modern quantum chemical methods to predict electronic circular dichroism spectra. *J Phys Chem A* 2003, 107:2524–2539.
94. Pecul M, Ruud K, Helgaker T. Density functional theory calculation of electronic circular dichroism using London orbitals. *Chem Phys Lett* 2004, 388:110–119.
95. Pecul M, Ruud K, Rizzo A, Helgaker T. Conformational effects on the optical rotation of alanine and proline. *J Chem Phys A* 2004, 108:4269–4276.
96. Frelek J, Kowalska P, Masnyk M, Kazimierski A, Korda A, Woznica M, Chmielewski M, Furche F. Circular dichroism and conformational dynamics of cepham and their carba and oxa analogues. *Chemistry* 2007, 13:6732–6744.
97. Grimme S, Mück-Lichtenfeld C. Calculation of conformational energies and optical rotation of the most simple chiral alkane. *Chirality* 2008, 20:1009–1015.
98. Wiberg KB, Wang Y, Wilson SM, Vaccaro PH, Jorgensen WL, Crawford TD, Abrams ML, Cheeseman JR, Luderer M. Optical rotatory dispersion of 2,3-hexadiene and 2,3-pentadiene. *J Chem Phys A* 2008, 112:2415–2422.
99. Tam MC, Crawford TD. Ab initio determination of optical rotatory dispersion in the conformationally flexible molecule (R)-epichlorohydrin. *J Chem Phys A* 2006, 110:2290–2298.
100. Mori T, Inoue Y, Grimme S. Time dependent density functional theory calculations for electronic circular dichroism spectra and optical rotations of conformationally flexible chiral donor–acceptor dyad. *J Org Chem* 2006, 71:9797–9806.
101. Mori T, Grimme S, Inoue Y. A combined experimental and theoretical study on the conformation of multiarmed chiral aryl ethers. *J Org Chem* 2007, 72:6998–7010.
102. Kondru RK, Wipf P, Beratan DN. Theory-assisted determination of absolute stereochemistry for complex natural products via computation of molar rotation angles. *J Am Chem Soc* 1998, 120:2204–2205.
103. Kondru RK, Wipf P, Beratan DN. Structural and conformational dependence of optical rotation angles. *J Chem Phys A* 1999, 103:6603–6611.
104. Mort BC, Autschbach J. Temperature dependence of the optical rotation of fenchone calculated by vibrational averaging. *J Chem Phys A* 2006, 110:11381–11383.
105. Woznica M, Kowalska P, Lysek R, Masnyk M, Gorecki M, Kwit M, Furche F, Frelek J. Stereochemical assignment of β -lactam antibiotics and their analogues by electronic circular dichroism spectroscopy. *Curr Org Chem* 2010, 14:1022–1036.
106. Neugebauer J, Jan Baerends E, Nooijen M, Autschbach J. Importance of vibronic effects on the circular dichroism spectrum of dimethyloxirane. *J Chem Phys* 2005, 122:234305 (7 pages).
107. Nooijen M. Investigation of Herzberg–Teller Franck–Condon approaches and classical simulations to include effects due to vibronic coupling in circular dichroism spectra: the case of dimethyloxirane continued. *Int J Quant Chem* 2006, 106:2489–2510.
108. Ruud K, Taylor PR, Åstrand P. Zero-point vibrational effects on optical rotation. *Chem Phys Lett* 2001, 337:217–223.
109. Mort BC, Autschbach J. Magnitude of zero-point vibrational corrections to optical rotation in rigid organic molecules: a time-dependent density functional study. *J Chem Phys A* 2005, 109:8617–8623.
110. Köppel H, Domcke W, Cederbaum LS. Theoretical investigation of Jahn-Teller and pseudo-Jahn-Teller interactions in the ammonia cation. *Adv Chem Phys* 1984, 57:59–246.
111. Dierksen M, Grimme S. A theoretical study of the chiroptical properties of molecules with isotopically engendered chirality. *J Chem Phys* 2006, 124:174301 (12 pages).
112. Demachy I, Ridard J, Laguitton-Pasquier H, Durnerin E, Vallverdu G, Archirel P, Lévy B. Cyan fluorescent protein: molecular dynamics, simulations, and electronic absorption spectrum. *J Phys Chem B* 2005, 109:24121–24133.
113. Bringmann G, Mühlbacher J, Repges C, Fleischhauer J. MD-based CD calculations for the assignment of the absolute axial configuration of the naphthylisoquinoline alkaloid dioncophylline A. *J Comput Chem* 2001, 22:1273–1278.
114. Brown A, Kemp CM, Mason SF. Electronic absorption, polarised excitation, and circular dichroism spectra of [5]-helicene (dibenzo[c,g]phenanthrene). *J Chem Soc A: Inorg Phys Theor* 1971:751–755.
115. Müller T, Wiberg KB, Vaccaro PH. Cavity ring-down polarimetry (CRDP): a new scheme for probing circular birefringence and circular dichroism in the gas phase. *J Chem Phys A* 2000, 104:5959–5968.

116. Kumata Y, Furukawa J, Fueno T. The effect of solvents on the optical rotation of propylene oxide. *Bull Chem Soc Jpn* 1970, 43:3920–3921.
117. Mukhopadhyay P, Zuber G, Goldsmith M, Wipf P, Beratan DN. Solvent effect on optical rotation: a case study of methyloxirane in water. *Chem Phys Chem* 2006, 7:2483–2486.
118. Warnke I, Ay S, Bräse S, Furche F. Chiral cooperativity and solvent-induced tautomerism effects in electronic circular dichroism spectra of [2.2]paracyclophane ketimines. *J Chem Phys A* 2009, 113:6987–6993.
119. Klamt A, Schüürmann G. COSMO: a new approach to dielectric screening in solvents with explicit expressions for the screening energy and its gradient. *J Chem Soc Perkin Trans* 1993, 2:799–805.
120. Klamt A, Jonas V. Treatment of the outlying charge in continuum solvation models. *J Chem Phys* 1996, 105:9972–9981.
121. Klamt A. The COSMO and COSMO-RS solvation models. *WIREs Comput Mol Sci* 2011, doi: 10.1002/wcms.56.
122. Cammi R, Tomasi J. Remarks on the use of the apparent surface charges (ASC) methods in solvation problems: iterative versus matrix-inversion procedures and the renormalization of the apparent charges. *J Comput Chem* 1995, 16:1449–1458.
123. Miertus S, Scrocco E, Tomasi J. Electrostatic interaction of a solute with a continuum. A direct utilization of ab-initio molecular potentials for the prevision of solvent effects. *Chem Phys* 1981, 55:117–129.
124. Tomasi J, Mennucci B, Cammi R. Quantum mechanical/continuum solvation models. *Chem Rev* 2005, 105:2999–3094.
125. Pecul M, Marchesan D, Ruud K, Coriani S. Polarizable continuum model study of solvent effects on electronic circular dichroism parameters. *J Chem Phys* 2005, 122:024106 (9 pages).
126. Guillaume M, Ruud K, Rizzo A, Monti S, Lin Z, Xu X. Computational study of the one- and two-photon absorption and circular dichroism of l-tryptophan. *J Phys Chem B* 2010, 114:6500–6512.
127. Bernasconi L, Blumberger J, Sprik M, Vuilleumier R. Density functional calculation of the electronic absorption spectrum of Cu[sup +] and Ag[sup +] aqua ions. *J Chem Phys* 2004, 121:11885–11899.
128. Brickell WS, Brown A, Kemp CM, Mason SF. π -electron absorption and circular dichroism spectra of [6]- and [7]-helicene. *J Chem Soc A* 1971, 756–760.
129. Crassous J, Rivera J, Fender NS, Shu L, Echegoyen L, Thilgen C, Herrmann A, Diederich F. Chemistry of C84: separation of three constitutional isomers and optical resolution of D2-C84 by using the “Bingel-Retro-Bingel” strategy. *Angew Chem Int Ed* 1999, 38:1613–1617.
130. Fanti M, Orlandi G, Poggi G, Zerbetto F. Semiempirical quantum-chemical assignment of the circular dichroism spectra of small chiral fullerenes. *Chem Phys* 1997, 223:159–168.
131. Furche F, Ahlrichs R. Absolute configuration of D2-symmetric fullerene C84. *J Am Chem Soc* 2002, 124:3804–3805.
132. Nomenclature and terminology of fullerenes: a preliminary survey. *Pure Appl Chem* 1997, 69:1411–1434.
133. Stephens PJ, Pan J, Devlin FJ, Urbanová M, Julínek O, Hájíček J. Determination of the absolute configurations of natural products via density functional theory calculations of vibrational circular dichroism, electronic circular dichroism, and optical rotation: the iso-schizozygane alkaloids isoschizogaline and isoschizogamine. *Chirality* 2008, 20:454–470.
134. Turbomole V6.2, Turbomole GmbH, Karlsruhe, 2011, www.turbomole.com
135. Łysek R, Borsuk K, Chmielewski M, Kałuża Z, Urbańczyk-Lipkowska Z, Klimek A, Frelek J. 5-dethia-5-oxacephams: toward correlation of absolute configuration and chiroptical properties. *J Org Chem* 2002, 67:1472–1479.
136. Furche F, Perdew JP. The performance of semilocal and hybrid density functionals in 3d transition-metal chemistry. *J Chem Phys* 2006, 124:044103–27.
137. Wang Y, Fleischhauer J, Bausch S, Sebastian M, Laur P. Conformational analysis and TDDFT calculations of the chiroptical properties of tris[1,2-propaneolato(2-)- κ O, κ O']-selenium/tellurium and related compounds. *Enantiomer* 2002, 7:343–374.
138. Jorge FE, Autschbach J, Ziegler T. On the origin of the optical activity in the d–d transition region of tris-bidentate Co(III) and Rh(III) complexes. *J Am Chem Soc* 2005, 127:975–985.
139. Stiefel EI, Brown GF. Detailed nature of the six-coordinate polyhedra in tris(bidentate ligand) complexes. *Inorg Chem* 1972, 11:434–436.
140. Mason SF. Optical activity and molecular dissymmetry in coordination compounds. In: *Fundamental Aspects and Recent Developments in Optical Rotatory Dispersion and Circular Dichroism*. London: Heyden and Son Ltd; 1973.
141. Hearson JA, Mason SF, Wood JW. The tris-(R)-(–)-propylenediamine complexes of rhodium(III). *Inorg Chim Acta* 1977, 23:95–96.
142. Jorge FE, Autschbach J, Ziegler T. On the origin of the optical activity in the d–d transition region of tris-bidentate Co(III) and Rh(III) complexes. *Inorg Chem* 2003, 42:8902–8910.